Investigation of the Variable Star CH Camelopardalis in the Planetary Nebula NGC 1501

Trent Mosher
Aisha Randhawa
Carolina Noviello
Adela Horsting
Kalée Tock
Stanford Online High School, Academy Hall Floor 2 8853, 415 Broadway, Redwood City, CA 94063; kaleeg@stanford.edu

Abstract   Time series images of the planetary nebula NGC 1501 were taken over several nights from the Las Cumbres Observatory robotic telescope network. Light curves of the central variable pre-white dwarf of NGC 1501, CH Cam, were derived using three different aperture photometry methods: image stacking on AstroImageJ, a custom Python program that used Source Extractor photometry, and a point spread photometry method. The light curves resulting from these photometric reductions were period-folded with multiple software routines including Skynet plotting, Astrosource, Period04, and Peranso. Approximately 30 prospective periods, ranging from 3 minutes to 110 minutes, were found. Some of these were similar to periods identified in previously-published literature, while others were not. Because CH Cam has been shown to have several pulsation modes, two pre-whitening methods—Period04 software and a custom Python sine-subtraction program—were also employed. Inconsistencies between periodograms resulting from the different photometric and analytic methods employed here, together with the low amplitude of the pulsations relative to the light of the background nebula and the expectation that these may vary with time, prevent us from drawing a firm conclusion about the pulsations of CH Cam.

1. Introduction

Commonly known as the Oyster Nebula, NGC 1501 (TIC 084306468) was discovered by William Herschel in 1787. It is characterized by its tetra-lobed ellipsoid shape (Sabbadin *et al.* 2000). Its central star, CH Camelopardalis (CH Cam), has coordinates 61.747487°, 60.920610° and parallax 0.5789 milliarcseconds, implying that it is a little over 1720 parsecs from Earth (Gaia Collab. *et al.* 2016; Babusiaux *et al.* 2023).

CH Cam is found in the instability strip on the Hertzsprung-Russell Diagram, to the left and above where white dwarf stars are found. It is classified as a GW Vir pulsating pre-white dwarf (pre-WD). GW Vir stars are recognized as having multi-periodic variations in luminosity with periods ranging from 300 to 6000 seconds, and are known to exhibit non-radial g modes (Córsico *et al.* 2019). Within CH Cam's classification as a pre-white dwarf, it is further described as a planetary nebula nucleus variable (PNNV) and a WCE or early-WC, which is a pulsating Wolf-Rayet with a dominant carbon line visual spectrum (Córsico *et al.* 2021; Ciardullo and Bond 1996). Specifically, it is classified as a WC4 star. CH Cam has $\log(T_{eff}) = 4.91 \pm 0.03$ and a surface chemical composition rich in helium, carbon, and oxygen (Bond *et al.* 1996).

Past research suggests that because of the current evolutionary stage of CH Cam, its pulsations likely change over a time scale of months. Not only is there is some expected variation in the magnitude and frequency with which the periods show up, but also, there is a possibility that some periodicities sometimes may not be present at all (Bond *et al.* 1996). Because of this variable star's location in the center of a planetary nebula, its small expected variations, and the fact that these may be changing with time, this target is particularly challenging.

CH Cam's variations were first detected by Ciardullo and Bond (1996), who found 10 periodicities between 1154 and 2000 seconds with low power spectrum amplitudes. Those authors used a software program called CLEAN (Roberts *et al.* 1987) to analyze the power spectrum, which demonstrated various low-frequency pulsation modes, as well as large variations in amplitude from one run to the next. These periods can be found in Table 1 (Bond *et al.* 1996). Later observations using 2019 TESS data detected 16 periods ranging between 1254 and 2077 seconds with amplitudes between 0.55 and 1.77 ppt (Córsico *et al.* 2021). This research used Fourier transforms and a customized pre-whitening tool with a 0.1% significance threshold to derive their variations.

Since the pixel size of the TESS telescope is large, it is useful to follow up TESS observations with images from ground-based telescopes that have smaller pixels, as is done in this work. Specifically, 218 images were taken across 7 different nights in late February and early March 2022 according to the target's window of visibility and our telescope time allotment. Each image was taken with a 150-second exposure time and a Johnson B filter. We did not have access to information on the characteristics of each night that images were taken, but the images we used were free of defects. Listed in Table 2 are the coordinates of CH Cam, and the comparison stars used in our research, which were chosen using the AAVSO's Variable Star Plotter (AAVSO 2022). The chosen comparison stars were the closest in the field in distance and in magnitude to the target star. Images for which the stars were blurry or the target was not centered were removed from the series.

This study employed three different photometries: AstroImageJ (AIJ; Collins *et al.* 2017), a Source Extractor module called via custom code written in Python (Bertin

Table 1. Bond *et al.* (1996) periods of CH Cam.

Period (s)	Period (minutes)	Amplitude (of Power Spectrum)
1154.36 ± 0.06	19.24	5.00 ± 0.37
1168.90 ± 0.18*	19.48	1.84 ± 0.37
1251.91 ± 0.13	20.87	2.66 ± 0.36
1251.91 ± 0.13	21.98	5.05 ± 0.36
1372.94 ± 0.22	22.89	1.87 ± 0.35
1431.53 ± 0.25	23.86	1.80 ± 0.36
1512.66 ± 0.28	25.21	1.77 ± 0.36
1760.73 ± 0.22	29.35	3.15 ± 0.36
1892.95 ± 0.32	31.55	2.55 ± 0.36
1999.16 ± 0.46	33.32	1.92 ± 0.36
5234.81 ± 1.62	87.25	3.73 ± 0.36

* *Possible alias (Bone* et al. *1996).*

Table 2. Target and comparison stars magnitudes and coordinates.

Name/Title	R.A. h m s	Dec. ° ' "	Mag. V	AAVSO AUID
CH Cam	04 06 59.2	60 55 15.6	14.4	000-BDH-360
Comp 1	04 07 31.35	60 57 38.8	14.081	000-BKG-698
Comp 2	04 07 07.12	60 59 48.3	14.314	000-BKG-699
Comp 3	04 07 39.90	60 57 48.7	14.758	000-BKG-700

and Arnouts 1996), and point spread photometry, which used processed images from Our Solar Siblings pipeline. The five methods of analysis employed in this paper are as follows:

1. 1-term Lomb Scargle AFTERGLOW software SKYNET plotting with the AIJ and SExtractor photometries.

2. PREWHITENING with the AIJ and SExtractor photometry through a custom code and PERIOD04 (Vanmunster 2004–2021).

3. Phase Dispersion Minimization with the psx photometry.

4. Astrosource's various algorithms including Lomb Scargle with the psx photometry.

5. PERANSO's CLEANest algorithm, which simultaneously searches for multiple periods, with the psx photometry.

In addition, we confirmed the results found in Córsico *et al.* (2021) for the 2019 TESS data, which used the PERIOD04 software.

1.1. Nyquist, Aliasing, and Spectral Window

Each of the 7 nights of data was sampled for a few hours at a cadence of about 162 seconds, or 2.7 minutes. Since these were sampled across multiple nights separated by random time intervals, our data count as nonuniform. As described in section 4.1 of VanderPlas (2018), such non-uniformity problematizes the application of the Nyquist frequency. Notably, "For unevenly sampled data, the truth is that the 'Nyquist limit'

might or might not exist, and even in cases where it does exist, it tends to be far larger (and thus far less relevant) than in the evenly sampled case" (VanderPlas 2018). For this reason, we do not consider our data to be compromised by the Nyquist limit.

Aside from Nyquist, other aliasing artifacts can arise. PERANSO's Spectral Window eliminates periods that are likely artifacts of sampling, which provides validation of the periods that it finds. In order to confirm our results, we used several period-finding methods such as PERSANSO and others on our data.

2. Instrumentation

The target star was imaged using 0.4-meter SBIG telescopes in Haleakala, Hawaii; MacDonald, Texas; and Teide, Spain, from the Las Cumbres Observatory Global Telescope network (Brown *et al.* 2013). The LCO network has standardized telescopes and cameras across all locations. The 218 images were taken with a SBIG STL 6303 camera. The camera has a format of 3K × 2K 9-micron, and a Field of View of 29.2 × 19.5 arcminutes. The pixel size used is 0.571 arcsecond/pixel. The files use 1 × 1 binning. The read noise is 14.5 e-, the gain is 1.6 ADU/e, and the dark current is 0.03 at 100° C.

3. ASTROIMAGEJ photometry

3.1. Description

A light curve showing all data from the ASTROIMAGEJ (AIJ) analysis was rendered using the PYTHON library called bokeh. plotting and is shown in Figure 1. AIJ performs differential aperture photometry, which involves measuring the flux of a target star relative to the combined flux of one or more comparison stars (Collins *et al.* 2017). The target star's relative flux is then calculated by dividing the target star's net integrated counts by the sum of the net integrated counts of all comparison stars. Net integrated counts represent the sum of all ADU counts within the aperture (after subtracting the average background flux between inner and outer annulus). The aperture size of 6 pixels (px), which was used for each reduction, was chosen manually because it enclosed the target while limiting the inclusion of the peripheral light of the nebula. The inner and outer radii of background annulus were set at 14 and 21 units,
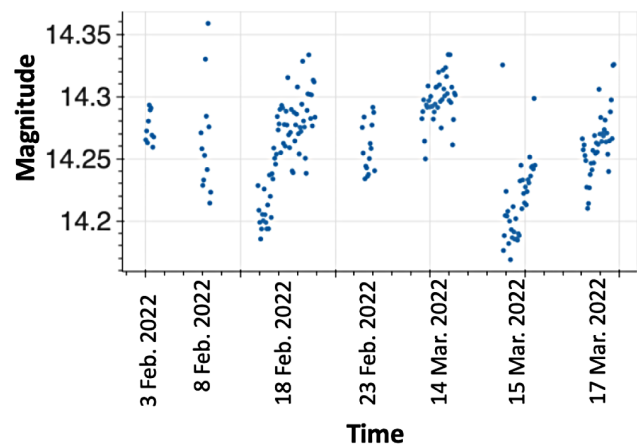

Figure 1. AIJ light curves for all 218 images used in this analysis.

respectively. The settings used on AIJ were accessed from the plot menu under seeing profile → multiple-aperture settings, and included default values of 1.5 for CCD gain, 9.5 for CCD readout noise, and 0.0 for CCD dark current per second.

Aperture photometry data for seven nights of images, totaling 218 images, were downloaded from AIJ into a spreadsheet. The following equation was used to convert the flux to calibrated magnitude:

$$Mag = -2.5 Log10\ (Flux) \qquad (1)$$

The instrumental magnitude was then added to the zero point for the telescope, resulting in the calibrated magnitude. Table 3 demonstrates the calculations to obtain calibrated magnitudes for CH Cam and comparison stars 1, 2, and 3 in the first image of Image Set 1.

The calibrated magnitude values for all 218 images and the corresponding Julian Dates were entered into the SKYNET plotting software for variable stars, AFTERGLOW (Reichart 2021). The three AFTERGLOW periodograms generated from separate calibration with each comparison star yielded five closely-matching prospective periods. Because the variation between periods found with each of the three comparison stars were negligible but Comp 3 showed the clearest peaks, only the five periods found using Comp 3 as seen in the periodogram in Figure 2 were inputted into the SKYNET period-folding algorithm. As shown in Figure 5, all five period folds demonstrated a subtle dip in magnitude and a sine wave-like form. Using DESMOS online graphing software, a sine wave was visually fitted to the calibrated target photometry and folded over a period of 89.84 minutes. This yielded an estimated amplitude of 0.037 magnitude, and is shown in Figure 3.

Because the form of the underlying sine wave from Figure 3 was difficult to approximate accurately, the average between each adjacent data point was calculated and plotted. This process was repeated three more times, which resulted in the more pronounced sine wave shown in Figure 4. A sine curve was then manually fitted to the data with more precision, resulting in a changed estimated amplitude of 0.0311 (in contrast with 0.037 as estimated with the non-averaged data). This suggests that the 89.84-minute period of CH Cam fluctuates 0.0311 in magnitude, mirroring data from the literature that detected similar low-amplitude pulsations.

This analysis suggests that the star CH Cam has five periods ranging from 84.56 to 110.54 minutes, shown in Figure 5. Of these periods, 84.56 and 89.61 minutes most closely correspond with the previous published period of 87.23 minutes. A list of these periods and their comparison to the periods found in the literature is shown in Table 4.

4. Source Extractor method

4.1. Data collection

To confirm the findings from AIJ, a second analysis was employed using Source Extractor (Bertin and Arnouts 1996), accessed through Google Colab and plotted using the Bokeh plotting library. The same 218 images were used in this method. In this process, it was found that Source Extractor was less

Table 3. Sample calculation of calibrated magnitude: first image.

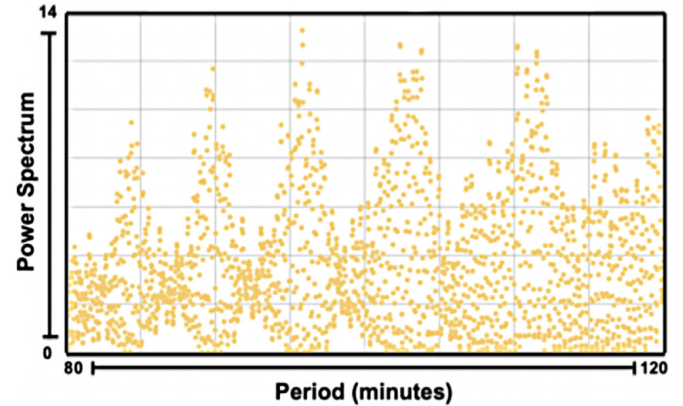| Image 1 Set 1	Netint Counts	Mag.	Zero Point	Calibrated Mag.
CH Cam	84006	−6.87	22.75	15.88
Comp 1	80307	−6.82	22.75	15.93
Comp 2	97501	−7.03	22.75	15.72
Comp 3	52657	−6.36	22.75	16.39

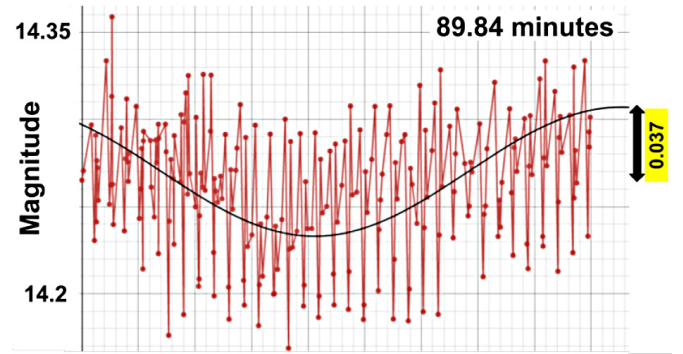Figure 2. AIJ periodogram from 0 to 120 minutes.

Figure 3. AIJ data period folded over 89.84 minutes and manually fitted with a sine curve. Estimated amplitude = 0.037.
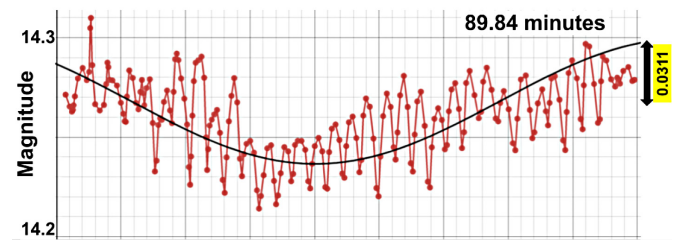

Figure 4. AIJ data period folded over 89.84 minutes with adjacent points averaged four times. Estimated amplitude = 0.0311.

dependent on aperture size than ASTROIMAGEJ was, as there was no difference in the periods found when the aperture size was adjusted. An aperture size of 6 pixels was used to match the previous analysis. In addition, to minimize variation by the comparison star chosen, the data points from each image for each comparison star were averaged. One outlier was identified and removed using lower and upper bounds as in Equation 2, which is sometimes called the Interquartile Range Method.

84.38 minutes

89.84 minutes

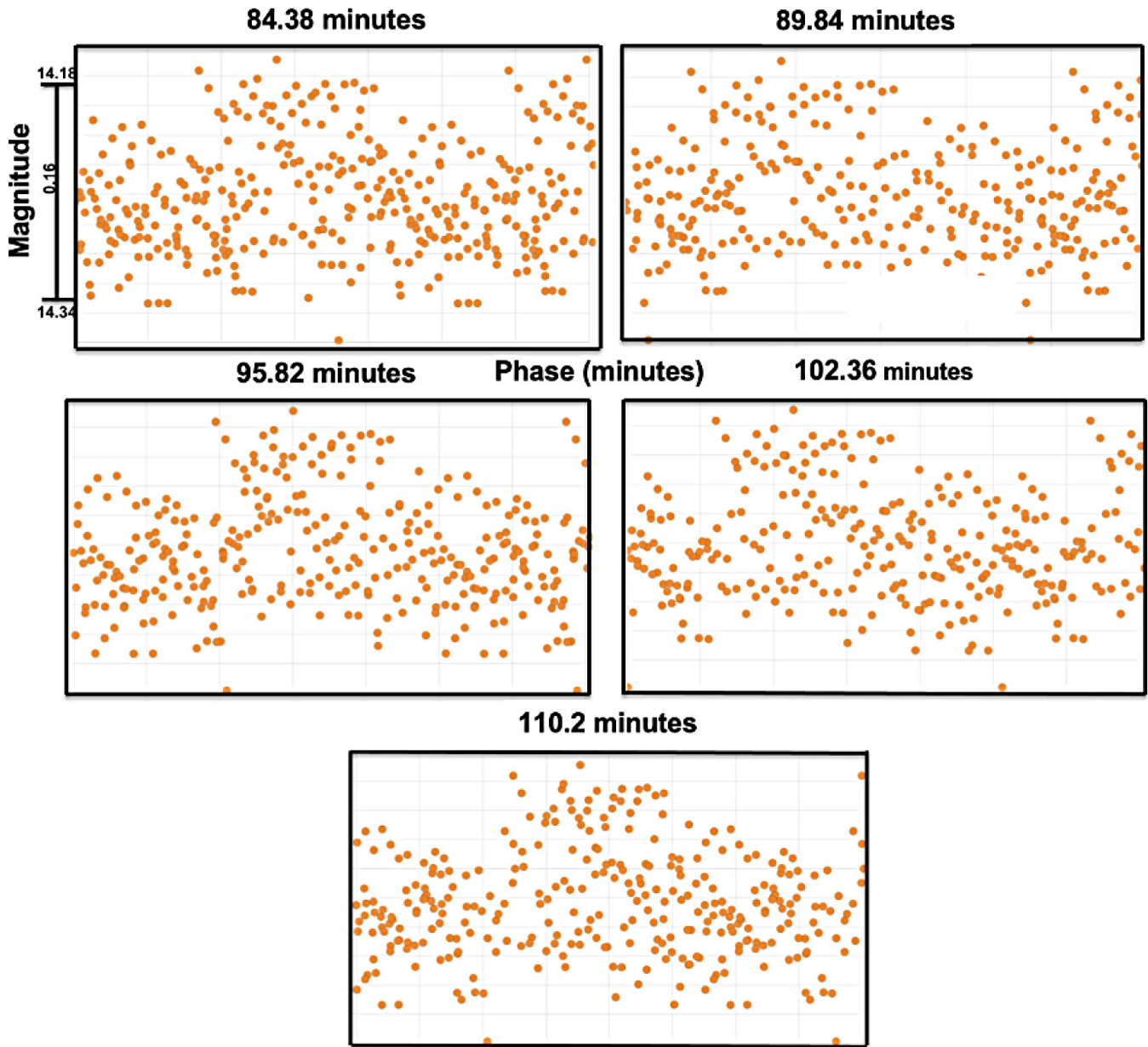## 95.82 minutes   Phase (minutes)   102.36 minutes

110.2 minutes

Figure 5. Period folded light curves using AstroImageJ Data. Five prospective periods (in minutes) from the first comparison star. As shown along the y-axis of the first graph, the curves displayed a variation in magnitude of about 0.16. Outliers were not excluded, as they made a negligible difference.
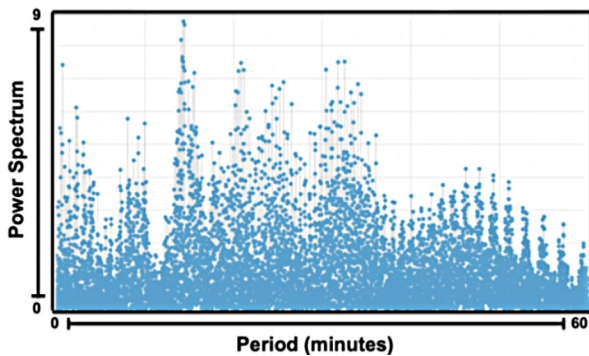

Figure 6. Skynet plotting Source Extractor periodogram from 0 to 60 minutes.

In this equation, Q_1 is the mean of the lower 50% of the data, Q_3 is the mean of the upper 50%, and R is the difference of $Q3 - Q_1$. Any data points that fell outside this bound were not included in the analysis.

$$B_{Lower} = Q_1 - 1.5\,R, \; B_{Upper} = Q_3 + 1.5\,R \qquad (2)$$

4.2. Periodograms

The calibrated SExtractor photometric measurements were folded through the "Variable" and "Pulsar" tabs of Skynet Plotting. The period-finding method employed by both these tabs is the one-term Lomb-Scargle periodogram as described by VanderPlas (2018). Although Lomb-Scargle is also cited as AIJ's period-folding method, the Skynet periodogram of the
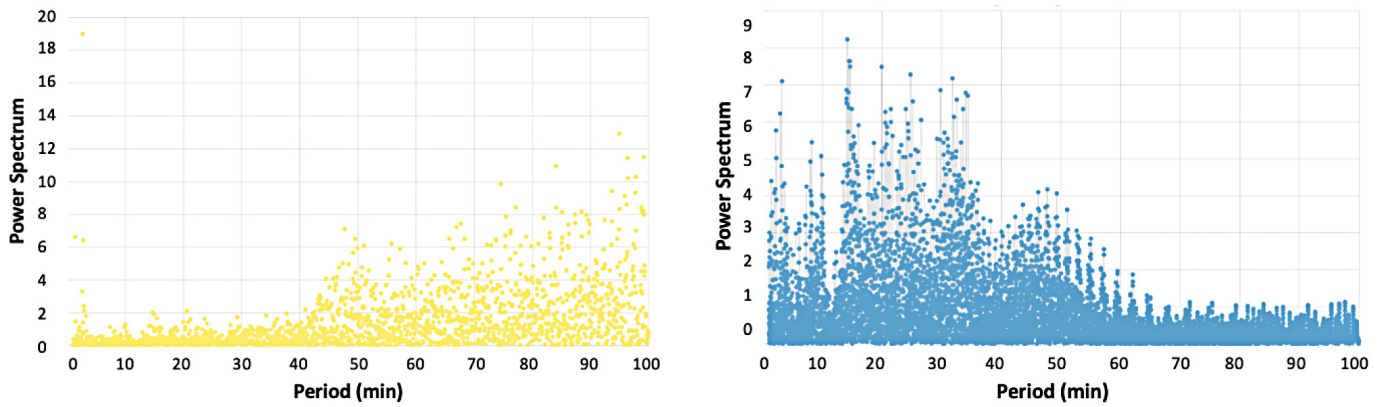
Figure 7. SKYNET plotting source extractor period folds for variable tab in SKYNET (left) and pulsar tab in SKYNET (right).
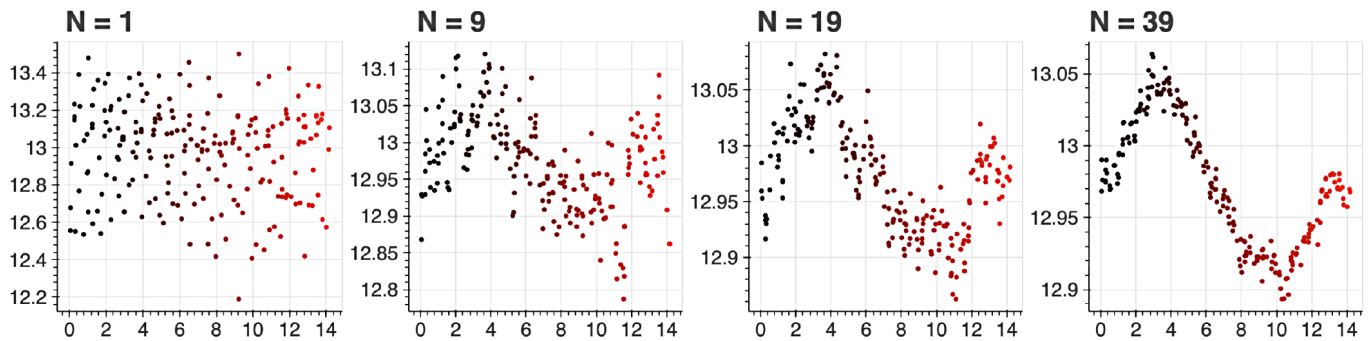

Figure 8. Different period folding graphs at period of 14.2029 by averaging adjacent points with different number of points N. Colormap: black to red, beginning of pulse to end.
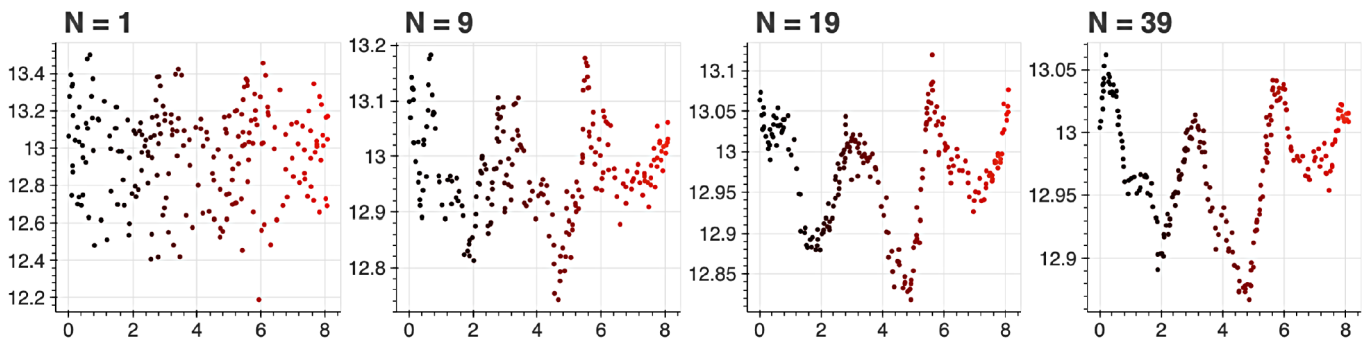

Figure 9. Different period folding graphs at period of 8.1264 by averaging adjacent points with different number of points N. Colormap: black to red, beginning of pulse to end.

SExtractor data did not resemble the AIJ periodogram. As shown in Figure 6, the AIJ periodogram peaks all occurred at periods longer than 80 minutes, while the SExtractor periodogram generated by the SKYNET pulsar tab showed peaks that all occurred at periods under 50 minutes. Note that to generate a variable star periodogram in the Pulsar section, it was necessary to subtract the timestamp of the first image from that of all subsequent images, convert the time of each data point into units of minutes, and specify the use of 0 bins, since data binning is a feature relevant to pulsars. In addition, calibration was set to 1.

When the Source Extractor photometry was initially folded in the respective "Variable" and "Pulsar" tabs, the periodograms made were rather different; see Figure 7 for this comparison. The "Variable" tab showed no noticeable peaks under 40

minutes and only noise above 40 minutes. The "Pulsar" tab did show many peaks, similar to those found in Bond *et al.* (1996). When the means of the data set from each of the seven nights were subtracted from each corresponding set, the SKYNET variable star tab's results became similar to those of the pulsar tab. This suggests that the pulsar tab's medium background subtraction algorithm, which is what differentiates the pulsar tab from the variable tab, might be optimal for variable stars with small periods, such as CH Cam.

4.3. Calculating amplitudes

PYTHON code was written to approximate the amplitudes of the pulsations found from the SExtractor photometry, smoothing the data by arithmetically averaging adjacent values. The value

9.8916 minutes

14.2029 minutes

21.1428 minutes

24.7604 minutes

30.4276 minutes

46.200 minutes

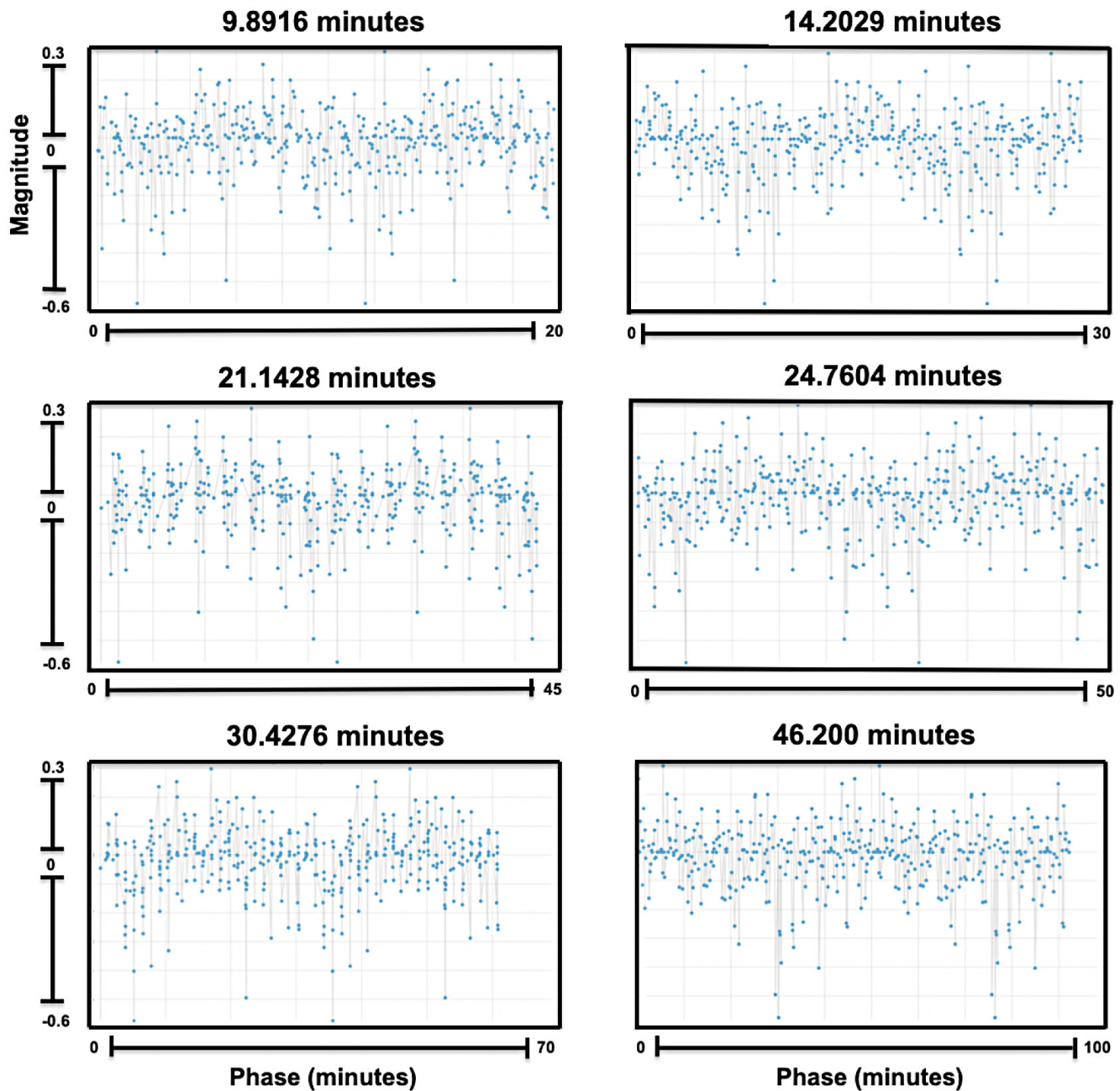**Phase (minutes)**   **Phase (minutes)**

Figure 10. SExtractor period folds.

N represents the number of adjacent points averaged. Using the method that will be described in section 5, the magnitudes of these newly muted pulsations were then corrected. Figures 8 and 9 show the use of this averaging technique. However, these pulsations were spurious because the overlap of the points used in adjacent averages causes the adjacent averages to be artificially similar to one another. This was confirmed by shuffling the data randomly and observing similar spurious pulsations. Therefore, this technique was only used to approximate amplitudes but not used to find periods.

4.4. Findings

Up to 16 different possible periods using the SExtractor data, which aligned between the pulsar tab and variable star tab,

were identified and are listed in full in Table 4. Examples of period folds can be found in Figure 10. Some periods were found to be close to half the value of some periods in Bond *et al.* (1996). Due to the properties of the Fourier transform, this is expected; the different period values that are a factor of 2 apart probably refer to the same pulsation.

5. Analyzing the effects of exposure time on magnitude

After finding a possible period of 2.878 minutes, it was necessary to see how much the magnitude found from period-folding was affected by the very close 2.5-minute exposure time. To model this, a simulation was coded on an online graphing calculator, Desmos. The simulation can be found at this url:

https://www.desmos.com/calculator/vlizyqjuvx.

To begin, assume that a star fluctuates with period T and amplitude A_{real}, over time x. This implies that the magnitude of the star can be modeled as in Equation 3:

$$F(x) = A_{real} \sin \left(\frac{2\pi}{T} x \right) \qquad (3)$$

We can allow the star to have an average magnitude of 0 for purposes of the simulation. Then assume that the images taken have an exposure of length E. Accordingly, the magnitude found in any photo from time x – E/2 to x + E/2 will be the average magnitude of F(x), which is F_{found}(x) in Equation 4:

$$F_{found} (x) = \frac{1}{E} \int_{x-E/2}^{x+E/2} F(t)\,dt \qquad (4)$$

Computing F_{found}(x) from the integral in Equation 4 and the definition of F(x) in Equation 3 we find Equation 5:

$$F_{found} (x) = \frac{A_{real}T}{E\pi} \sin \left(\frac{\pi E}{T} \right) \sin \left(\frac{2\pi}{T} \right). \qquad (5)$$

After imaging with exposure E, the period will not have changed, we can take the amplitude of F_{found}(x) and find Equation 6:

$$A_{imaged} = \frac{A_{real}T}{\pi E} \sin \left(\frac{\pi E}{T} \right). \qquad (6)$$

From this equation one can use A_{imaged} to approximate the true amplitude of the star's variations. If T >> E or when E tends to 0, it is not necessary to use this approximation. By using this equation, the amplitudes of high-frequency pulsations are sometimes found to be slightly higher then when they are estimated by folding the data.

6. Prewhitening

6.1. Introduction

Prewhitening is a method for finding more pulsations of a variable star, if the star has more than one simultaneous pulsation. The method is performed by finding the most likely pulsation, fitting a curve to that pulsation (usually a sine curve), and then using the parameters of that sine curve to subtract that found pulsation out of the data. This new data set is then analyzed again in the same manner, finding pulsations, subtracting them such that the data become cleaner every time a pulsation is subtracted. The goal in performing this analysis is to try to decrease the error in the periods found, and possibly find more periods as the data set becomes clearer.

6.2. PERIOD04

PERIOD04 software is a prewhitening tool, performing the same prewhitening algorithm described above, and is adapted to work with time series containing gaps (Lenz and Breger 2005). It employs three different tabs to perform a prewhitening analysis: Time String (to record periods), Fit (to calculate the statistical significance of periods), and Fourier (to get a periodogram). Both the ASTROIMAGEJ photometry and Source Extractor photometry were input into the PERIOD04 software.

The frequencies were extracted using the procedure outlined under the "Tutorial 2: Least-Squares fitting of data including a periodic time shift" (page 58 of the PERIOD04 User Guide). Eight periods were found with the ASTROIMAGEJ photometry and 14 were found with the Source Extractor photometry. Most periods found in each method were rather similar to those found earlier, except for a few periods ranging from 50 to 75 minutes. The fits were obtained by simultaneously fitting the periods to the data. See Table 4 for a list of these periods. The significance of these periods was calculated by the software. Most significances for the ASTROIMAGEJ photometry were around 0.002 and those of the Source Extractor photometry were around 10^{-6}. We stopped running the software when it recommended that the periods it found were no longer significant (which was around $0.005\,\sigma$).

6.3. PYTHON PREWHITENING code

In an attempt to ascertain greater confidence in the periods found by Source Extractor, we also wrote a code that would subtract the sine curves out of the dataset, which was used as part of a pre-whitening method in tandem with the periodogram by SKYNET.

The code first folded the data around the period found by SKYNET. Then, to attain a more confident sine fit, it averaged each data point with the 49 that surrounded it (centered around each data point). Then, because this is analogous to taking an exposure, the correction derived in section 5 was used to better approximate the amplitude. In addition, instead of just using the period that was suggested by SKYNET, four more periods at $\pm 0.0006\%$ and $\pm 0.0012\%$ the suggested period were tried. An example is shown in Figure 11. These percentages were chosen based on some testing which showed that these numbers made slightly better fits in some cases, while staying within the peaks in the periodograms from SKYNET. Then, the PYTHON library called SCIPY was used to determine the best fit of a sine curve across all the five total averaged period folds.

After the parameters of this sine curve were found, we subtracted the sine curves out of the original, un-averaged data set, and then confirmed through testing that the corresponding period was absent from the periodogram.

This method found many more periods than Source Extractor, as after more and more periods were subtracted out of the data set, more would appear. Most of the periods that arose were below the periodogram amplitude of spurious periods that arose by randomly shuffling the Source Extractor data around and running them through SKYNET. Therefore, no periods found by this method are reported here.
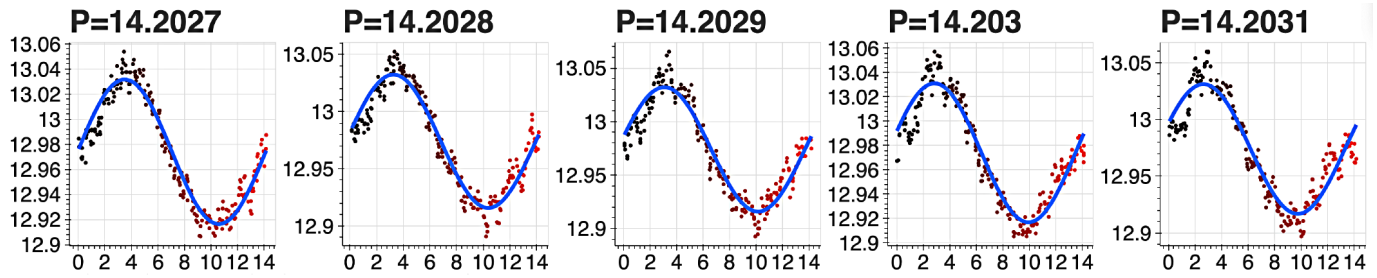
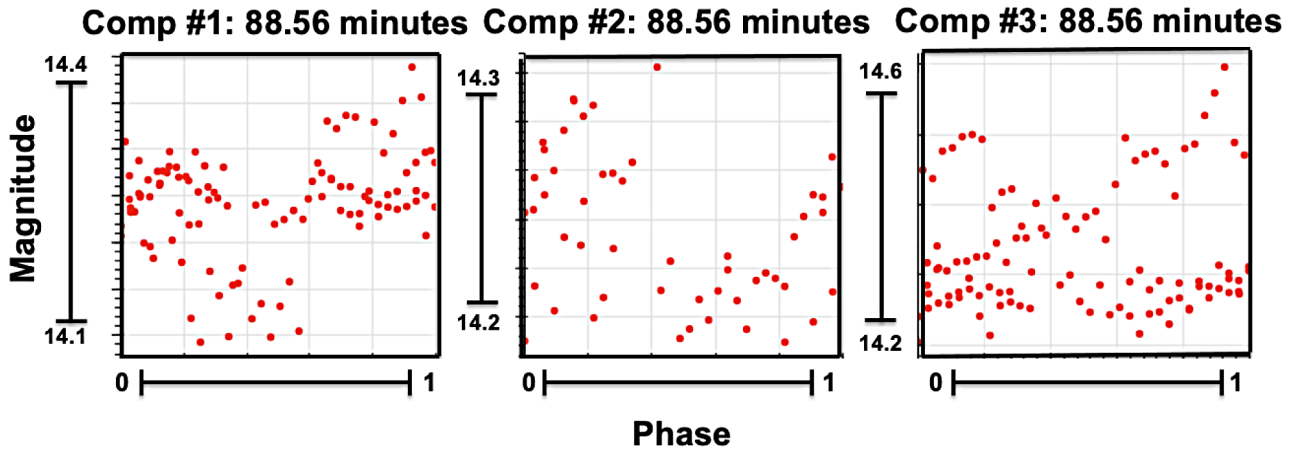Figure 11. Five different sine fits for small differences in periods P.

Figure 12. psx Photometry: The different period folds for each comparison star at a period of 88.56 minutes.
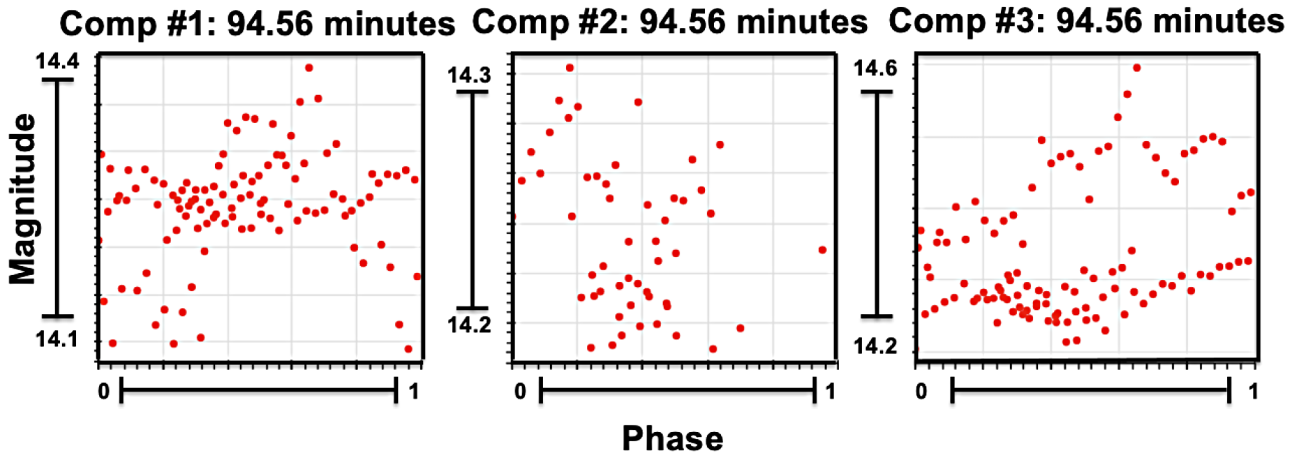

Figure 13. psx Photometry: The different period folds for each comparison star at a period of 94.56 minutes.

7. psx method

Another attempted method of analysis was psx photometry (Bertin and Arnouts 1996). This method uses a point spread function to identify stars and measure their magnitudes. Using this photometry, we were unable to confirm any of the periods found in the literature, nor any of the periods we had found using the AstroImageJ method or the Source Extractor method. We wrote a Python code to use the data returned by the Our Solar Siblings pipeline and period-fold for any period of input. Our 218 images were used for this method in addition to some archival data from previous LCO observations of this nebula. No conclusive periods were found from this method.

In the end, this method ended up containing messier data than those derived from the AIJ and Source Extractor methods; both Figures 12 and 13 show how different the period folds for two sample periods looked between each of the three comparison stars. The second comp star was not found in all the images, which explains why there are visually fewer data points for that plot. The dissimilarity of the plots renders this method inconclusive and in need of further investigation.

8. Peranso

Peranso (Vanmunster 2004–2021) is a light curve and period analysis software that is able to run CLEANest (Foster 1995)
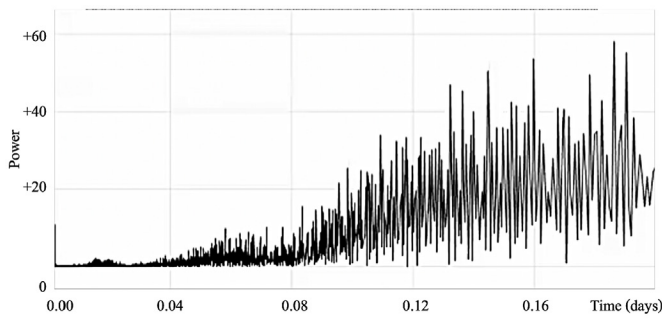
Figure 14. Peranso CLEANest periodogram on this study's data and a few other points from the LCO archive.
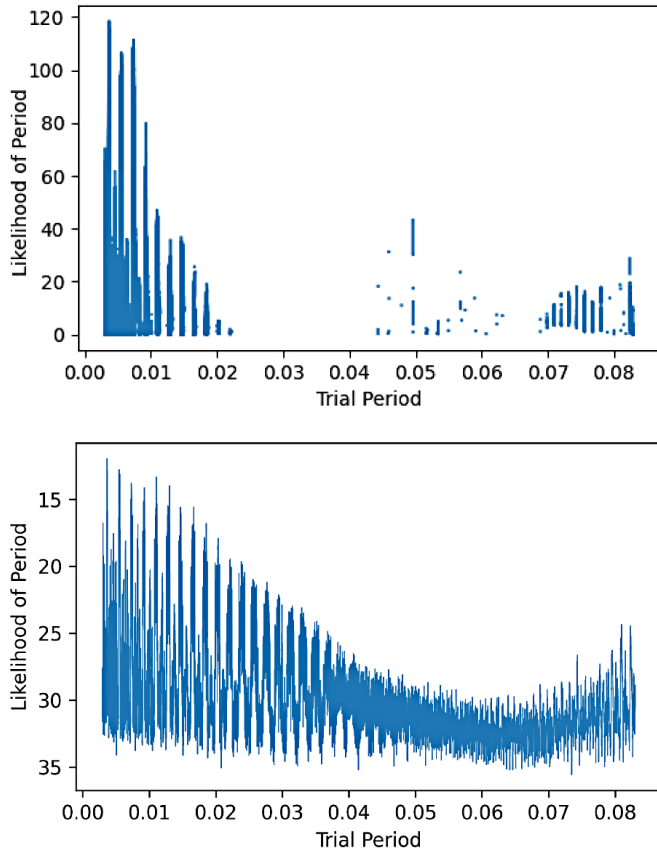

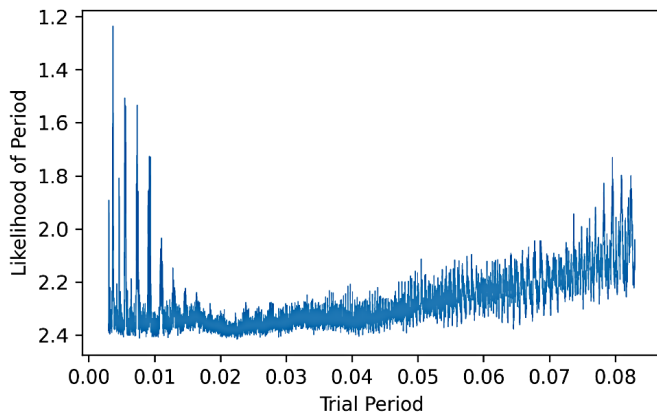Figure 15. (Upper) ANOVA periodogram. (Lower) String PDM Periodogram.

Figure 16. PDM periodogram.

analysis. This software was used with the assistance of Michael Fitzgerald to see whether CLEANest would be able to more accurately find the many pulsations of CH Cam. However, the main periods found were much larger than expected for this type of star. The data used were a compilation of our 218 images data collected from Las Cumbres Observatory, along with a few other data points from the past ten years that had used the same filter and captured CH Cam. As shown in Figure 14, the clearest peak in the periodogram was close to the sampling frequency, suggesting an alias.

9. Astrosource

For further analysis of the psx method, we used Astrosource, a software developed by Michael Fitzgerald (Fitzgerald *et al.* 2021). To use the software, the psx photometry from the OSS Pipeline was used as the input. To search for comparison stars, the code first uses the list of stars and compares the variance of each star's flux, as the standard deviation, to each other star. Then it eliminates the stars that had higher variance. This repeats until the optimal comparison stars are found. After calibrating with those comps, it uses various methods to compute the most probable periods, including ANOVA, harmonic ANOVA, Phase Dispersion Minimization (PDM), and Lomb Scargle (VanderPlas 2018; Dworetsky 1983). PDM and String are similar, in that they both attempt to minimize the distribution of a binned data, either by calculating the distance between the points in flux-phase space or by their standard deviation. Figures 15 and 16 show the likelihood plots for ANOVA, String, and PDM. The archival LCO images along with our 218 images were used in this method.

For Lomb Scargle, up to six summations of sine curves were output by the software, as shown in Figure 17. However, including more than three terms is not justified given the constraints of the system, and from visual inspection, additional terms do not improve the fit. In addition, the one-term Lomb-Scargle did not find a good fit. The two- and three-term Lomb-Scargle fits looked better, but these used almost negligible second and third sinusoidal terms. Given that they fitted the data to essentially one sine curve, this pulsation should have been found by the one-term fit. In addition, the period listed by the two-term and three-term Lomb-Scargle fits was around 5.37 minutes, which is almost exactly twice as long as the sampling frequency, suggesting a possible alias. The hypothesis that this is an alias is substantiated by the fact that Peranso did not find a period of that length, and Peranso takes into account the Spectral Window, as described in the Introduction; see section 1.1

10. TESS data analysis

As part of our process to verify the results of our analysis methods, we tried to replicate the analysis and results found in the 2019 paper using the same TESS data (Córsico *et al.* 2021). A complete download of the TESS data for NGC 1501, released in 2018, was found in the MAST observatory portal. In the 2019 paper, the analysis was done using pre-whitening that was done through the authors' customized tool (Córsico

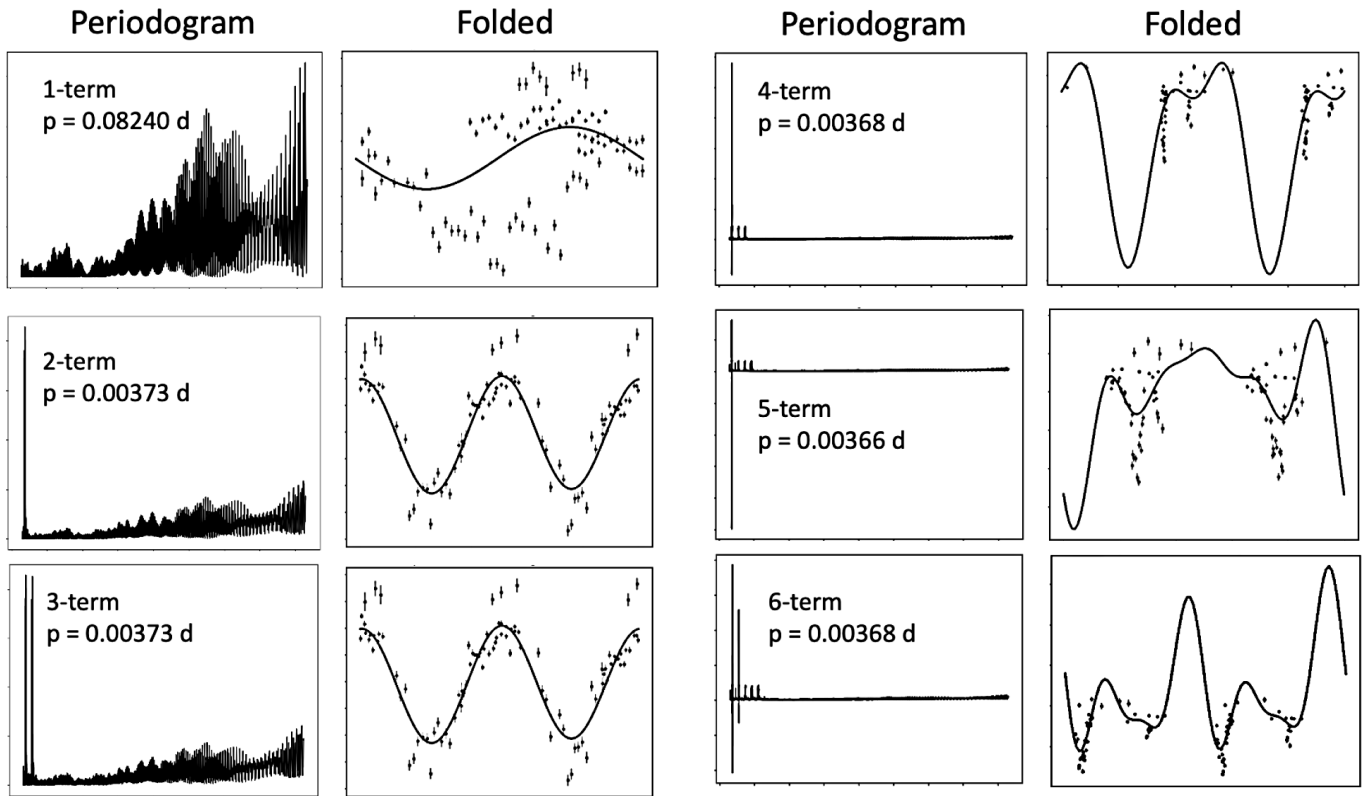| Periodogram	Folded	Periodogram	Folded

Figure 17. The different period folds for each comparison star at a period of 94.56 minutes.
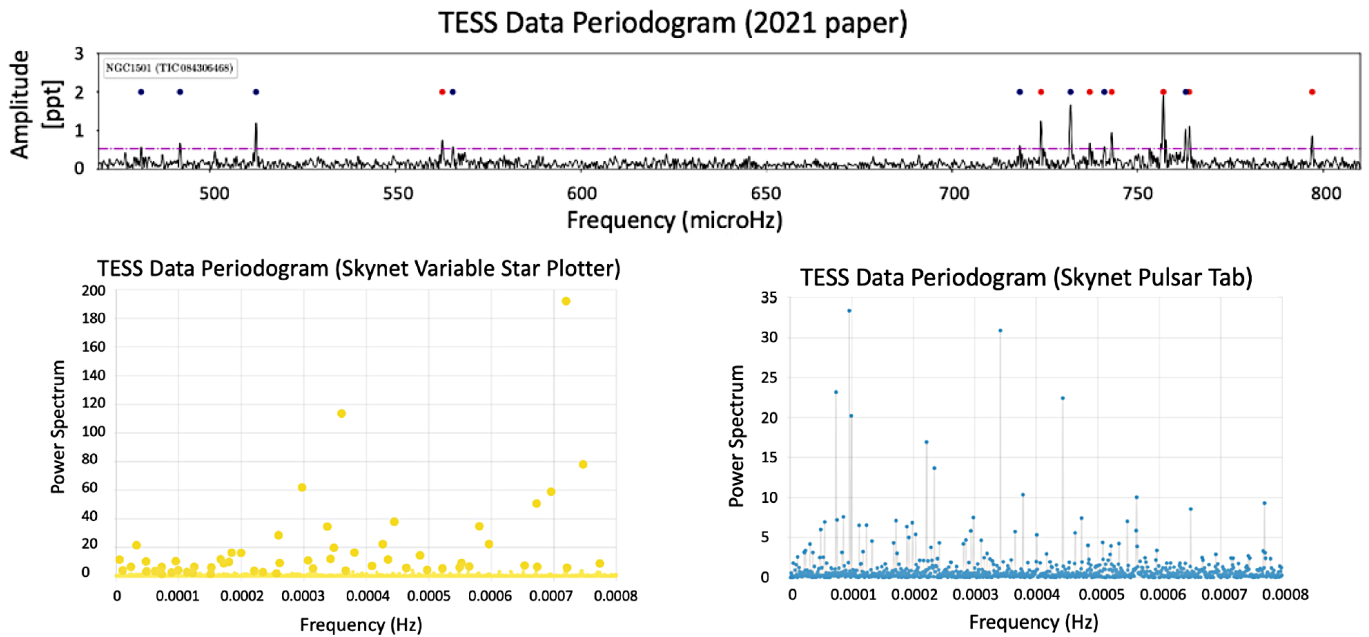

Figure 18. Comparison of TESS data periodograms.

et al. 2021). We ran these data through Skynet plotting—both the Pulsar and Variable Star tabs (see section 4.2)—as well as through Period04 (see section 6.2).

10.1. Skynet plotting

In applying the TESS data to both Skynet's variable star plotter and its Pulsar tool, the initial light curve of the data

aligned with that of Figure 2 in Córsico *et al.* (2021). Neither periodogram from the Skynet Pulsar or Variable Star tabs confidently matched the periodogram given in Córsico *et al.* (2021); see Figure 18. However, some similarities were found. Peaks were found around 650–800 μHz in the Skynet Variable Star tab, which could align with the periods found in that same range by Córsico *et al.* (2021). It is likely that the discrepancies

that arose were due to the differences in our methods of analysis using Skynet and the customized method used in Córsico *et al.* (2021). Further investigation would be helpful to verify the validity of the analysis of our own results and of past results.

10.2. Period04

The same TESS data were run in Period04, and were able to reproduce 10 of 11 periods that were found in Córsico *et al.* (2021) within about ± 0.1 second in all cases; see column 5 in Table 4. This suggests that the results from Period04 discussed in section 6.2 were valid. Four additional periods were found. It is likely that any of the small discrepancies in results are due to the custom nature of their tool.

11. Conclusion

After performing several different methods—AstroImageJ, Source Extractor, psx, Astrosource, Prewhitening, and Peranso—about 30 periods were found, shown in Table 4. Six of the periods found using the AstroImageJ and SExtractor methods are rather close to historical periods, while about three are close to the half values of historical periods. Reduction of our data via psx, Astrosource, and Peranso did not confirm pulsations in CH Cam, while Prewhitening with the Period04 software and our custom code both confirmed these periods and found additional ones. In accordance with the expectation that this phase in stellar evolution of pre-white dwarfs is expected to change over short time periods, it is possible that in the time since some of the historical periods were calculated, particularly those in the Bond paper, the periods of CH Cam have changed. Some inconsistencies among the results of the various period finding methods employed here as well as the complexity of CH Cam suggest that further research would be helpful in the investigation of this star.

12. Acknowledgements

References

AAVSO. 2022, Variable Star Plotter (https://www.aavso.org/apps/vsp/).

Babusiaux, C., *et al.* 2023, *Astron. Astrophys.*, **674A**, 32 (DOI: 10.1051/0004-6361/202243790, arXiv:2206.05989).

Bertin, E., and Arnouts, S. 1996, *Astron. Astrophys., Suppl. Ser.*, **117**, 393 (DOI: 10.1051/aas:1996164).

Bond, H. E., *et al.* 1996, *Astron. J.*, **112**, 2699 (DOI: 10.1086/118214).

Brown, T. M., *et al.* 2013, *Publ. Astron. Soc. Pacific*, **125**, 1031 (DOI: 10.1086/673168).

Córsico, A. H., Althaus, L. G., Miller Bertolami, M. M., and Kepler, S. O. 2019, *Astron. Astrophys. Rev.*, **27**, 7 (DOI: 10.1007/s00159-019-0118-4).

Córsico, A. H., *et al.* 2021, *Astron. Astrophys.*, **645A**, 117 (DOI: 10.1051/0004-6361/202039202).

Ciardullo, R., and Bond, H. E. 1996, *Astron. J.*, **111**, 2332 (DOI: 10.1086/117967).

Collins, K. A., Kielkopf, J. F., Stassun, K. G., and Hessman, F. V. 2017, *Astron. J.*, **153**, 77 (DOI: 10.3847/1538-3881/153/2/77).

Dworetsky, M. M. 1983, *Mon. Not. Roy. Astron. Soc.*, **203**, 917 (DOI: 10.1093/mnras/203.4.917).

Fitzgerald, M. T., Gomez, E., Salimpour, S., Singleton, J., and Wibowo, R. W. 2021, *J. Open Source Software*, **6**, 2641 (DOI: 10.21105/joss.02641).

Foster, G. 1995, *Astron. J.*, **109**, 1889.

Gaia Collaboration, *et al.* 2016, *Astron. Astrophys.*, **595A**, 1 (DOI: 10.1051/0004-6361/201629272).

Lenz, P., and Breger, M. 2005, *Comun. Asteroseismology*, **146**, 53 (DOI: 10.1553/cia146s53).

Reichart, D. E. 2021, *Phys. Teacher*, **59**, 728 (DOI: 10.48550/arXiv.2103.09895).

Roberts, D. H., Lehar, J., and Dreher, J. W. 1987, *Astron. J.*, **93**, 968.

Sabbadin, F., Benetti, S., Cappellaro, E., and Turatto, M. 2000, *Astron. Astrophys.*, **361**, 1112 (DOI: 10.48550/arXiv.astro-ph/0007039).

VanderPlas, J. T. 2018, *Astrophys. J., Suppl. Ser.*, **236**, 16 (DOI: 10.3847/1538-4365/aab766).

Vanmunster, T. 2004–2021, Peranso v.2.50 light curve and period analysis software (http://www.cbabelgium.com/peranso).